ACS APPLIED MATERIALS & INTERFACES

Research Article

www.acsami.org

Biodegradable Protein-Based Rockets for Drug Transportation and Light-Triggered Release

Zhiguang Wu, Xiankun Lin, Xian Zou, Jianmin Sun,* and Qiang He*

State Key Laboratory of Robotics and System (HIT), Academy of Fundamental and Interdisciplinary Sciences, Harbin Institute of Technology, Harbin 150080, China

Supporting Information

ABSTRACT: We describe a biodegradable, self-propelled bovine serum albumin/poly-L-lysine (PLL/BSA) multilayer rocket as a smart vehicle for efficient anticancer drug encapsulation/delivery to cancer cells and near-infrared light controlled release. The rockets were constructed by a template-assisted layer-by-layer assembly of the PLL/BSA layers, followed by incorporation of a heat-sensitive gelatin hydrogel containing gold nanoparticles, doxorubicin, and catalase. These rockets can rapidly deliver the doxorubicin to the targeted cancer cell with a speed of up to 68 μm/s, through a combination of biocatalytic bubble propulsion and magnetic guidance. The photothermal effect of the gold nanoparticles under NIR irradiation enable the phase transition of the gelatin hydrogel for rapid release of the loaded doxorubicin and efficient killing of the surrounding cancer cells. Such biodegradable and multifunctional protein-based microrockets provide a convenient and efficient platform for the rapid delivery and controlled release of therapeutic drugs.

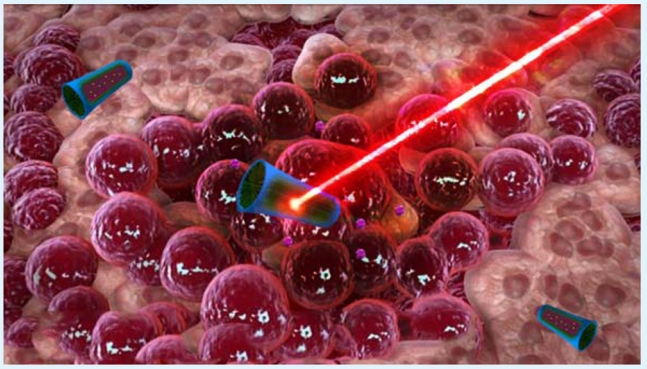

KEYWORDS: *layer-by-layer, autonomous propulsion, rocket, biodegradation, drug release*

INTRODUCTION

The development of synthetic motors capable of converting chemical energy into autonomous movement is one of the most exciting challenges in the field of nanotechnology.[1−5] Various synthetic motors propelled by different mechanisms have been developed during the past decade.[6−12] Among them, functionalized rolled-up or polymeric-based microengines,[13,14] bimetallic nanorods,[15] Janus particles,[16] helical swimmers,[17−19] ultrasound-propelled nanomotors,[20,21] particle-based motor,[22,23] polymer multilayer-based rockets, or Janus capsule motors[24,25] have displayed impressive performance in various potential applications, ranging from biomedicine to environmental analysis and remediation.[26] This tiny nanodevices have the capability of picking-up, transport, and release diverse cargoes including polymeric particles, cancer cells, nucleic acids, bacteria, and oil droplets.[27−31]

Practical applications of synthetic motors in biomedical fields require both its degradation into nontoxic compounds and high biocompatibility with living organisms. However, previously reported synthetic motors commonly consist of noble metals or synthetic polymers with poor biocompatibility and biodegradability, limiting thus their practical applications.[32−34] Recently, a biodegradable plant-based microswimmer has been reported, but its ability for drug delivery applications have yet to be demonstrated[35] Hence, the development of biodegradable synthetic motors capable of the transport and release of cargoes in a controlled manner is still a challenging issue.

A promising strategy to fabricate biocompatible and biodegradable functionalized motors is based on the template-assisted layer-by-layer (LbL) assembly.[24,25] The LbL-template method involves consecutive assembly of different components, such as natural or synthetic polymers, proteins, lipids, vesicles, micelles, and nanoparticles, into the pores of membrane templates, without altering the active properties of such components.[35−39] As a natural polymer, proteins have outstanding biocompatibility and biodegradability, thus they are widely used as building units for the preparation various drug carriers. For example, LbL assembled protein nanotubes have been developed recently as enzymatic bioreactors and biosensors for biomedicine and bioseparations.[40] However, the use of nanotubes based on a protein-based framework as autonomous motor system has not been reported yet.

Here we demonstrate the successful fabrication of a biodegradable poly-L-lysine hydrochloride/bovine serum albumin multilayer microtube through the use of the nanoporous template-assisted LbL technique, following the integration of a thermal-sensitive gelatin hydrogel into the multilayer tubes. Unlike the traditional hollow multilayer tube, this gelatin hydrogel core can greatly improve the encapsulation capacity,

Received: September 3, 2014
Accepted: December 12, 2014
Published: December 12, 2014

Scheme 1. Fabrication and Light-Triggered Drug Release Process of $(PLL/BSA)_{10}$-DOX-CAT-AuNPs-Gelatin Rockets: (a) Deposition of Different Functional Components into the PLL/BSA Multilayer Coated Template; (b) Release of $(PLL/BSA)_{10}$-DOX-CAT-AuNPs-Gelatin Rockets by Dissolving the Template; (c) Anticancer Drug (DOX) Release from the Rockets under Near-Infrared (NIR) Laser Irradiation

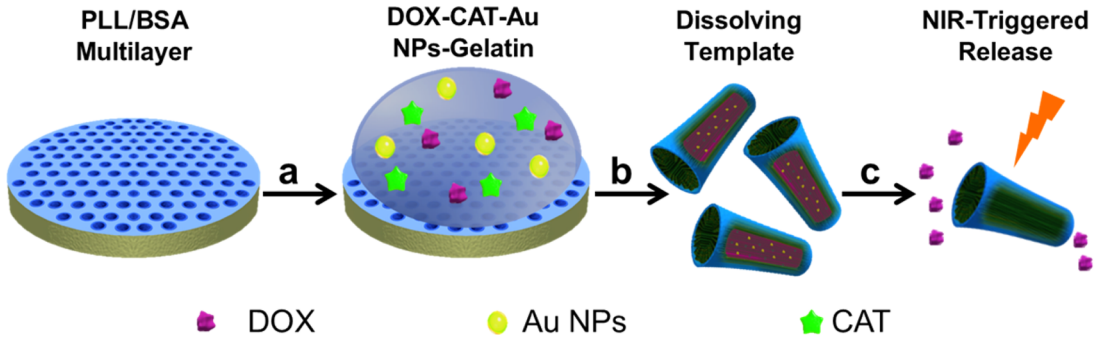

thus loading different functional components such as catalase (as catalyst for autonomous propulsion), gold nanoparticles (for photothermal phase transition of the hydrogel), and doxorubicin (anticancer drug). The free diffusion of hydrogen peroxide fuel into the catalase containing gelatin hydrogel results in the catalytic generation of water and oxygen bubbles ("propulsion gas"), that are expelled through the large opening of the microtubes, moving thus the tube forward ("miniaturized rocket"). The combination of low melting point gelatin (melting point of about 36.5 °C) and gold nanoparticles with a strong plasmon resonance in the near-infrared (NIR) region allow for a fast drug release. Upon NIR irradiation, electromagnetic energy is absorbed by the gold nanoparticles and dissipated as heat into the gelatin hydrogel. The increase in temperature inside the microengines will result in theof the gelatin hydrogel melting and subsequently the rapid release of the encapsulated drugs into the surrounding media. In addition, the protein-based rockets can be enzymatically degraded after completing their task, and thus will not cause adverse and toxic effects in vivo. This represents a new concept on the use of proteins as building blocks for the development of biocompatible self-powered synthetic engines for practical biomedical applications.

EXPERIMENTAL SECTION

Materials. Unless otherwise noted, all the chemicals were obtained from commercial suppliers and used without further purification. Doxorubicine (DOX) was purchased from Shanghai Yuanye Biological Technology Co., Ltd.. Gelatin, catalase (CAT), bull Bovine serum albumin (BSA), poly-L-lysine hydrochloride (PLL, M_w = 30 000–70 000), $HAuCl_4 \cdot 4H_2O$, citric acid monohydrate, H_2O_2 (30% v/v), NaCl, and ethanol were used without further purification. Water purified using a Milli-Q purification system (18.2 MΩ cm^{-1}) was used in all the experiments.

Preparation of Gold Nanoparticles (AuNPs). To prepare citrate-stabilized gold nanoparticles, 50 mL of a citric acid (2.2 mM) solution was placed in a three-neck round-bottom flask and heated to 100 °C. Subsequently, 1 mL of 25 mM $HAuCl_4$ solution was added and the reaction mixture was heated at 100 °C for 3.5 min before it was allowed to cool to room temperature.

Preparation of $(PLL/BSA)_{10}$-DOX-CAT-AuNPs-Gelatin Rockets. The $(PLL/BSA)_{10}$-DOX-CAT-AuNPs-gelatin rockets were fabricated through a template assisted Layer-by-Layer assembly protocol. Polycarbonate (PC) membranes (average pore diameter, 5 μm), were employed as the templates. The PLL solution (1 mg/mL in 0.1 M NaCl) and BSA solution (1 mg/mL) were used for the assembly of PLL/BSA multilayers in the inner pores of the template. All the solutions were filtered through a 0.45 μm-membrane filter before use. The negatively charged BSA and positively charged PLL were alternately adsorbed for 30 min in the pores of the membrane for the formation one bilayer. Between each layer growing, the membrane was washed three times with purified water before immersing the template into the next polyelectrolyte solution. When 10 bilayers of polymer film were obtained, the template was immersed into the mixture solution containing AuNPs, DOX (1 mg/mL), catalase (1 mg/mL), and gelatin (25 mg/mL). The solution and template were incubated in a vacuum jar at 50 °C for 30 min. Then, the template was kept at 4 °C overnight. In order to remove the excess of polyelectrolyte and gel layers, the top and bottom surface of the membrane template were polished using a wet cotton swab. Subsequently, the rockets were released by dissolving the membrane in CH_2Cl_2. The resulting solution was washed 3 times with CH_2Cl_2. The rockets were collected by centrifugation at 4000 g for 3 min, followed by redispersion in ethanol and water. The rocket solution was then stored at 4 °C for further experiments.

Biodegradation of the Protein Rockets. The protein rockets were incubated overnight with α-chymotrypsin solution (5 U mL^{-1}) in phosphate buffer solution (PBS) at pH 7.4, at room temperature. The samples were then separated from the incubation solution and washed three times with water before SEM characterization.

Cell Culture and Investigation. The standard trypsin protocol was performed to cultivate the HeLa cells in a Petri dish. The cell lines were incubated in dulbecco's modified eagle medium (DMEM) containing 10% fetal calf serum and 1% penicillin and streptomycin at 37 °C, in a 5% CO_2 atmosphere.

RESULTS AND DISCUSSION

The fabrication process and light-activated drug release of the protein-based rockets are illustrated in Scheme 1. The framework of 10 bilayers of positively charged poly-L-lysine hydrochloride (PLL) and negatively charged bovine serum albumin (BSA) were first deposited onto a track-etched porous polycarbonate (PC) membrane (10 μm thickness, pore diameter 5 μm) following a previously reported procedure.[36] Then, the thermal-sensitive gelatin hydrogel cores were incorporated into the rockets by immersing the template in a aqueous solution containing gelatin, catalase (CAT), gold nanoparticles (AuNPs), and doxorubicin (DOX) under vacuum at 40 °C, followed by cooling the coated templates at 4 °C, transforming the gelatin solution into a semi/solid hydrogel structure. Well-dispersed $(PLL/BSA)_{10}$-DOX-CAT-AuNPs-gelatin rockets solutions were obtained after dissolution of the PC template in CH_2Cl_2 and the washing steps mentioned in the previous section.

To verify the presence of BSA in the building wall of the rockets, we employed fluorescein isothiocyanate labeled BSA

dx.doi.org/10.1021/am507680u | ACS Appl. Mater. Interfaces 2015, 7, 250–255

(FITC-BSA) during the rockets fabrication. Figure 1A shows the confocal laser scanning microscopy image of $(PLL/BSA)_{10}$-DOX-CAT-AuNPs-gelatin rockets. A green florescent region is clearly observed on the surface of the rockets, corresponding to the FITC-BSA layer, thus confirming its presence. The red florescent area is the intrinsic fluorescence of the loaded DOX. The intensity distribution of a single rocket in the red channel (Figure 1B) shows that the maximum florescent intensity comes from the framework of the rocket, and the fluorescence intensity decreases close to the axis of the rocket, indicating that the rocket was not fully blocked by the gelatin hydrogel. The SEM image in the Supporting Information, Figure 1, shows the top view of a rocket with hollow conical structure. The wall thickness of the rocket is within the range of 400−600 nm, which is larger than that of the tubes with the same number of bilayers and similar components,[41] suggesting the successful integration of the gelatin hydrogel into the rocket. This method of loading DOX into the rockets by using the natural protein hydrogel should also be available to the encapsulation of other drug molecules with high water solubility and low molecular weight.[42] TEM image in Figure 1C (see also the Supporting Information, Figure 1A) show the top view structure of a $(PLL/BSA)_{10}$-DOX-CAT-AuNPs-gelatin rockets. These images further confirm that the rockets are fully loaded with the gelatin hydrogel. Also, the thin pieces near the opening of the rocket indicate the presence of a high population of AuNPs in the hydrogel. The enlarged TEM image (the inset one in Figure 1C) shows the aggregation of AuNPs inside the rocket. The UV−vis spectra in Figure 1d shows the red shifts of the plasmon resonance absorption peak before loading of the AuNPs at 522 nm and after the AuNPs were loaded into the hydrogel at 660 nm further confirming the aggregation of AuNPs and its successful incorporation into the gelatin hydrogel. Interestingly, the maximum absorption peak of the aggregated AuNP is close to the NIR region, which is essential for the NIR irradiation and assisted photothermal DOX release. Light in the near-infrared (NIR) region is attractive in the context of biomedical applications because body tissue has the highest transmissivity in this region (so-called biological window).

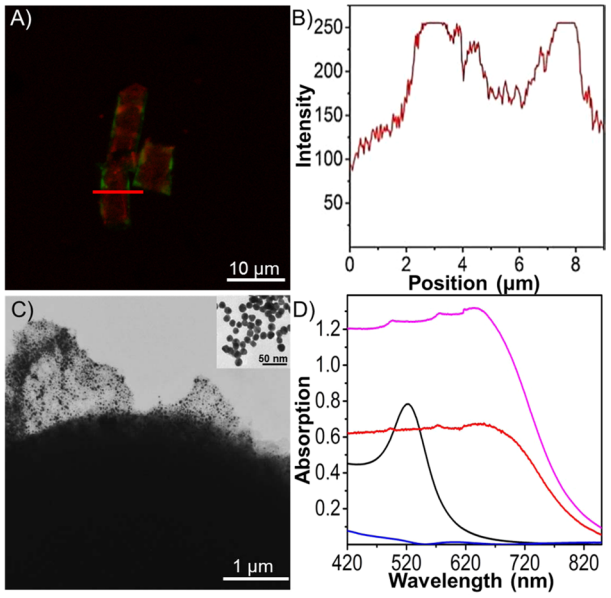

Figure 1. (A) Confocal laser scanning microscopy images and (B) corresponding fluorescence intensity profile of $(PLL/BSA)_{10}$-DOX-CAT-AuNPs-gelatin rockets. (C) TEM images of $(PLL/BSA)_{10}$-DOX-CAT-AuNPs-gelatin rockets. Inset shows the TEM image corresponding to AuNPs in the gelatin hydrogel. (D) UV−vis spectra of AuNPs (black curve), the gelatin (blue curve), the suspension of gelatin and AuNPs (red curve), and the hydrogel of gelatin with AuNPs (pink curve), respectively.

Because of the main components of the $(PLL/BSA)_{10}$-DOX-CAT-AuNPs-gelatin rockets being proteins and polypeptides, the rockets can be easily degraded by enzymes normally present in the human body. To evaluate the biodegradability of rockets, α-chymotrypsin, a digestive enzyme present in human pancreatic juice, was evaluated.[43] The rockets were incubated with α-chymotrypsin in PBS buffer (pH 7.4) overnight. The SEM images in Figure 2 show the protein-based rockets before and after the enzymatic treatment. A clear rocket structure can be observed in Figure 2A, however, after incubation with the enzyme as shown in Figure 2B, the rockets collapsed into tiny thin pieces. This is because α-chymotrypsin can catalytically cleave peptide amide bonds of the proteins and the peptides present on the rockets, losing thus its conical structure. It should be indicated here the completed degradation of these protein-based rocket is only completely achieved after several days of enzymatic treatment. Such a long period of time allows for the successful drug delivery and release by the rockets. Therefore, the biodegradability of the rockets could benefit their metastasis after releasing the encapsulated drugs and reduce the adverse effect in vivo. This feature makes these rockets attractive for practical drug delivery and release in the human body.

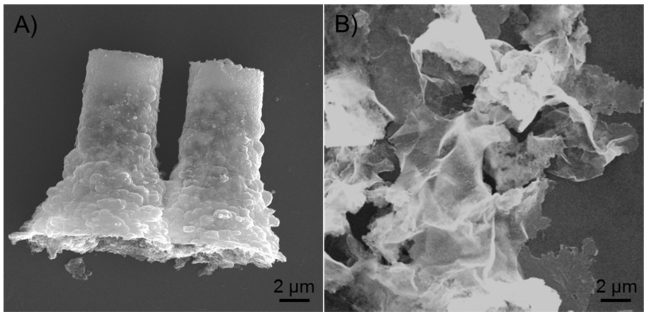

Figure 2. SEM images of the $(PLL/BSA)_{10}$-DOX-CAT-AuNPs-gelatin rockets before (A) and after (B) incubating with the α-chymotrypsin solution.

Practical motion-based drug delivery applications require that effective motor propulsion is maintained at physiological temperature. For instance, the Supporting Information Figure 2 and the corresponding Video 1 in the Supporting Information illustrate the movement of a $(PLL/BSA)_{10}$-DOX-CAT-AuNPs-gelatin rocket at the speed of around 4 μm/s at 0.5% H_2O_2 at 37 °C. These images show a long trail of microbubbles, catalytically generated on the inner space and released from the rear of the microtube. The propulsion of the $(PLL/BSA)_{10}$-DOX-CAT-AuNPs-gelatin rockets relies on the ejection of the oxygen bubbles generated from the biocatalytic decomposition of hydrogen peroxide (H_2O_2) by catalase present inside the hydrogel at physiological temperature. The protein-based rockets containing the gelatin hydrogel can still allow for the diffusion of H_2O_2. Most interior space of the gelatin hydrogel network inside the rockets is filled by the solvent, which favors

the diffusion of H_2O_2 into the catalase active sites and the release of oxygen bubbles. Similar to previous reports,[10,25] the speed of rockets is linearly dependent on the H_2O_2 concentration, increasing from 4 μm/s at 0.5% H_2O_2 to 59 μm/s at 2.0% H_2O_2 at 37 °C (see the Supporting Information, Figure 3). As a result, the drag force could be estimated by using the Einstein−Stoke equation according to our previous work,[24] and thus the drag force of rocket at a speed of 59 μm/s is nearly 7 pN. Such speeds are faster than the speed of a well-known linear motor kinesin (roughly 800 nm/s),[44] but lower than the catalase propelled rolled-up or template microengines at similar conditions.[45,46] This can be partially attributed to the encapsulation process of the catalase into the gelatin hydrogel, which decreases the interaction of catalase and H_2O_2.[47] The average speed of the rockets at 37 °C is substantially higher than that at room temperature because of the higher activity of catalase at physiological temperature.[48] At hydrogen peroxide concentrations higher than 5%, the rockets display a short lifetime (less than 10 min) because of the inactivation of the catalase by the presence of a high gradient of hydroxyl radicals.[49]

The anticancer drug loaded rocket also demonstrates effective propulsion in cell culture media for drug transportation to the predefined cancer cells. The remote navigation of the rockets to the predefined cell site can be achieved by assembling negatively charged magnetic nanoparticles (average size of 10 nm) into the rocket by electrostatic attraction and by theuse of an external magnetic field. The time-lapse images in Figure 3, taken from the Supporting Information, Video 2,

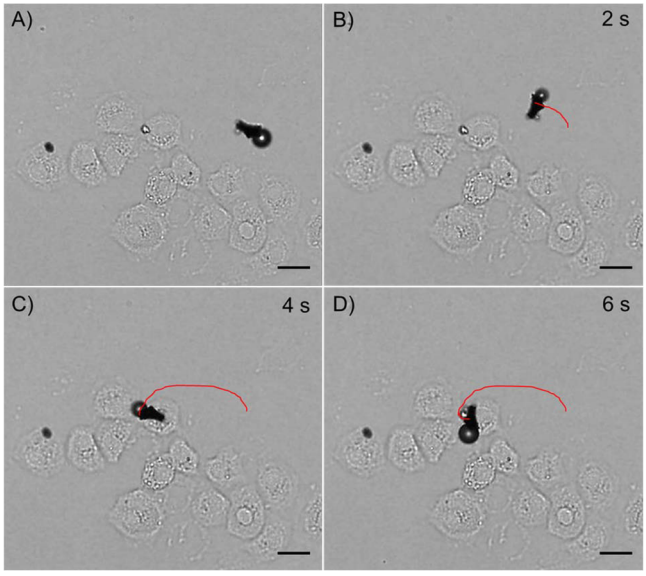

Figure 3. (A−D) Time-lapse images of the movement of a $(PLL/BSA)_{10}$-DOX-CAT-AuNPs-gelatin rockets to the sheets of Hela cells in PBS solution with 0.5% H_2O_2 at 37 °C. Scale bar = 20 μm.

illustrate a $(PLL/BSA)_{10}$-DOX-CAT-AuNPs-gelatin rocket rapidly moving to the targeted cancer cells under navigation of an external magnetic field at 0.02 T. It has been proved that this magnetic intensity can only change the direction of motion, but cannot influence its speed.[13] Initially, the rocket moved randomly at a speed of 4 μm/s in the cell culture media (pH 7.2) containing 0.5% H_2O_2 at 37 °C (Figure 3A, B). Such speed is slower than that in pure PBS solution, reflecting the increased viscosity in cell culture media and the fouling of cell culture to the rockets.[50] Subsequently, the rocket was steered to approach the targeted HeLa cells by applying a magnetic field (Figure 3C). Upon contacting HeLa cells, the rocket attached onto the surface of cells and did not detach because of the electrostatic absorption between the cell membrane and the front end of the multilayer rockets (Figure 3D). Also, the penetration of the moving rockets into the outer membrane of the HeLa cells should partially contribute to its immobilization. At this low concentration of peroxide fuel, the HeLa cells did not change their shape for more than 90 min, implying the survival of HeLa cells. If needed, the rockets could utilize biocompatible fuel or apply fuel-free propulsion to ensure in vivo viability with human cells.[10,51]

Recent study has shown the tubular micromotors (diameter, 2 μm; length, 20 μm), which loaded SiO_2 and Au particles for the delivery and autonomous release of cargos.[52] Similarly, the biodegradable protein-based motor can also perform the NIR-response drug release, the rockets release the aggregate containing DOX as drug cargo under the exposure of NIR beam. The optical microscopy time-lapse images in Figure 4,

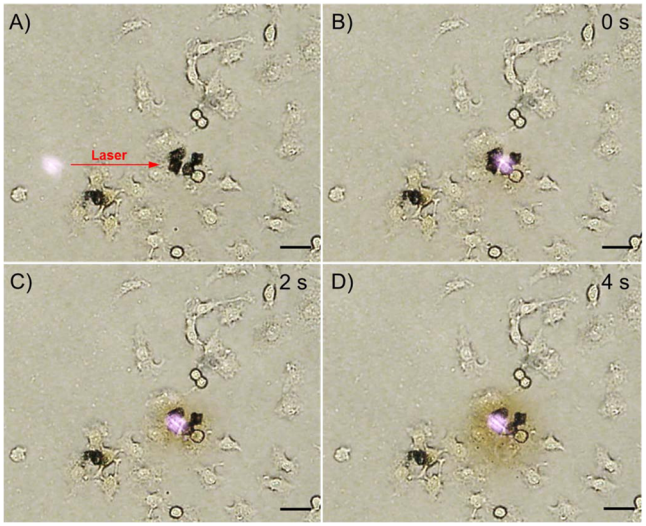

Figure 4. (A−D) Time-lapse images of triggering the DOX release from the $(PLL/BSA)_{10}$-DOX-CAT-AuNPs-gelatin rockets under NIR irradiation. The purple spot shows the NIR laser, whereas the brown solution indicates the DOX released from rockets. Scale bar = 20 μm.

taken from the Supporting Information, Video 3, show the NIR-triggered DOX release from the $(PLL/BSA)_{10}$-DOX-CAT-AuNPs-gelatin rockets attached to HeLa cells. The DOX cargos, clearly observed in the figure in brown color, rapidly diffuses into the surrounding media after NIR irradiation. The diffusion of DOX colored solution into the surrounding media reach values of up to 5000 μm^2 in 4 s. Negligible observation of particles released from the rocket, indicates the size of DOX cargo possess nanoscale during the diffusion to nearby cells. It should be noted that the brown color region observed in the optical microscope correspond to a relatively high concentration of DOX (1 ng per rocket). At lower DOX concentration, as testified by the fluorescence images in the Supporting Information Figure 4, the brown coloration cannot be clearly observed after the NIR irradiation for 1 s, although effective NIR triggered release was achieved. This is mainly because these rockets were loaded with a relatively low amount of DOX (0.2 ng per rocket). The NIR-triggered DOX cargo

release is attributed to the photothermal effect imparted by the AuNPs present in the gelatin hydrogel. The AuNPs in the hydrogel could convert light energy to heat energy and causes the gel−sol phase transformation of the gelatin hydrogel and the subsequent release of the encapsulated DOX.[53] These results confirm the possibility of using protein-based rockets as a biodegradable and multifunctional drug carrier autonomous vehicle. It is worth mentioning that nanoporous template-assisted layer-by-layer (LbL) technique allows for the construction of tubular nanostructure with controllable geometry, size and thickness ranging from tens of nanometers to several hundreds of nanometers. Therefore, protein-based nanorockets with defined sizes at the nanoscale could be conveniently prepared for future practical applications.

CONCLUSIONS

In conclusion, we have demonstrated a hybrid protein-based rocket for drug delivery and light-triggered drug release in a controlled manner. The rockets can be completely biodegraded after enzymatic treatment under physiological conditions, thus indicating minimal in vivo toxicity. The hydrogel cores allows for a high amount of drugs encapsulated in the rockets, with only a slight reduction in its speed. The newly developed protein-based rockets can be conveniently navigated to the targeted sites with the release of the encapsulated drug triggered under biocompatible NIR irradiation. Our strategy of integrating a heat-sensitive hydrogel into the rockets, allows for the efficient and the controllable loading of various components with different sizes of hydrophobic or hydrophilic properties. Such biodegradable protein-based rockets can serve as a convenient and efficient platform for next generation of smart vehicles in the biomedical field.

ASSOCIATED CONTENT

Supporting Information

Experimental section and additional figure and videos. This material is available free of charge via the Internet at http://pubs.acs.org

AUTHOR INFORMATION

Corresponding Authors

*E-mail: sunjm@hit.edu.cn.

*E-mail: qianghe@hit.edu.cn.

Notes

The authors declare no competing financial interest.

ACKNOWLEDGMENTS

We thank Dr. Wei Gao for discussion and Dr. Beatriz Jurado-Sanchez to polish the language. This work was supported by the National Nature Science Foundation of China (91027045 and 21103034), the Fundamental Research Funds for the Central Universities, China Postdoctoral Science Foundation funded project, and State Key Laboratory of Robotics and System (HIT).

REFERENCES

(1) Schroeder, A.; Heller, D. A.; Winslow, M. M.; Dahlman, J. E.; Pratt, G. W.; Langer, R.; Jacks, T.; Anderson, D. G. Treating Metastatic Cancer with Nanotechnology. *Nat. Rev. Cancer* **2012**, *12*, 39−50.

(2) Wang, J. *Nanomachines: Fundamentals and Applications*, 1st ed; Wiley−VCH: Weinheim, Germany, 2013.

(3) Mei, Y. F.; Solovev, A. A.; Sanchez, S.; Schmidt, O. G. Rolled-up Nanotech on Polymers: From Basic Perception to Self-Propelled Catalytic Microengines. *Chem. Soc. Rev.* **2011**, *40*, 2109−2119.

(4) Mallouk, T. E.; Sen, A. Powering Nanorobots. *Sci. Am.* **2009**, *300*, 72−77.

(5) Wang, H.; Zhao, G.; Pumera, M. Beyond Platinum: Bubble-Propelled Micromotors Based on Ag and MnO_2 Catalysts. *J. Am. Chem. Soc.* **2014**, *136*, 2719−2722.

(6) Wilson, D. A.; Nolte, R. J. M.; van Hest, J. C. M. Autonomous Movement of Platinum-Loaded Stomatocytes. *Nat. Chem.* **2012**, *4*, 268−274.

(7) Gao, W.; Sattayasamitsathit, S.; Orozco, J.; Wang, J. Highly Efficient Catalytic Microengines: Template Electrosynthesis of Polyaniline/Platinum Microtubes. *J. Am. Chem. Soc.* **2011**, *133*, 11862−11864.

(8) Mou, F.; Chen, C.; Ma, H.; Yin, Y.; Wu, Q.; Guan, J. Self-Propelled Micromotors Driven by the Magnesium Water Reaction and Their Hemolytic Properties. *Angew. Chem., Int. Ed.* **2013**, *52*, 7208−7212.

(9) Gao, W.; Wang, J. Synthetic Micro/Nanomotors in Drug Delivery. *Nanoscale* **2014**, *6*, 10486−10494.

(10) Wilson, D. A.; Nijs, B.; de Blaaderen, A.; van Nolte, R. J. M.; van Hest, J. C. M. Fuel Concentration Dependent Movement of Supramolecular Catalytic Nanomotors. *Nanoscale* **2013**, *5*, 1315−1318.

(11) Loget, G.; Kuhn, A. Electric Field-Induced Chemical Locomotion of Conducting Objects. *Nat. Commun.* **2011**, *2*, 535.

(12) Li, J.; Zhang, J.; Gao, W.; Huang, G.; Di, Z.; Liu, R.; Wang, J.; Mei, Y. Dry-Released Nanotubes and Nanoengines by Particle-Assisted Rolling. *Adv. Mater.* **2013**, *25*, 3715−3721.

(13) Soler, L.; Magdanz, V.; Fomin, V. M.; Sanchez, S.; Schmidt, O. G. Self-Propelled Micromotors for Cleaning Polluted Water. *ACS Nano* **2013**, *7*, 9611−9620.

(14) Gao, W.; Uygun, A.; Wang, J. Hydrogen-Bubble-Propelled Zinc-Based Microengines in Strongly Acidic Media. *J. Am. Chem. Soc.* **2012**, *134*, 897−900.

(15) Paxton, W. F.; Kistler, K. C.; Olmeda, C. C.; Sen, A.; St. Angelo, S. K.; Cao, Y.; Mallouk, T. E.; Lammert, P. E.; Crespi, V. H. Catalytic Nanomotors: Autonomous Movement of Striped Nanorods. *J. Am. Chem. Soc.* **2004**, *126*, 13424−13431.

(16) Gao, W.; Pei, A.; Feng, X.; Hennessy, C.; Wang, J. Organized Self-Assembly of Janus Micromotors with Hydrophobic Hemispheres. *J. Am. Chem. Soc.* **2013**, *135*, 998−1001.

(17) Kim, S.; Qiu, F.; Kim, S.; Ghanbari, A.; Moon, C.; Zhang, L.; Nelson, B. J.; Choi, H. Fabrication and Characterization of Magnetic Microrobots for Three-dimensional Cell Culture and Targeted Transportation. *Adv. Mater.* **2013**, *25*, 5863−5868.

(18) Schamel, D.; Mark, A. G.; Gibbs, J. G.; Miksch, C.; Morozov, K. I.; Leshansky, A. M.; Fischer, P. Nanopropellers and Their Actuation in Complex Viscoelastic Media. *ACS Nano* **2014**, *8*, 8794−8801.

(19) Venugopalan, P. L.; Sai, R.; Chandorkar, Y.; Basu, B.; Shivashankar, S.; Ghosh, A. Conformal Cytocompatible Ferrite Coatings Facilitate the Realization of a Nanovoyager in Human Blood. *Nano Lett.* **2014**, *14*, 1968−1975.

(20) Garcia-Gradilla, V.; Orozco, J.; Sattayasamitsathit, S.; Soto, F.; Kuralay, F.; Pourazary, A.; Katzenberg, A.; Gao, W.; Shen, Y.; Wang, J. Functionalized Ultrasound-Propelled Magnetically Guided Nanomotors: Toward Practical Biomedical Applications. *ACS Nano* **2013**, *7*, 9232−9240.

(21) Wang, W.; Castro, L. A.; Hoyos, M.; Mallouk, T. E. Autonomous Motion of Metallic Microrods Propelled by Ultrasound. *ACS Nano* **2012**, *6*, 6122−6132.

(22) Dong, B.; Zhou, T.; Zhang, H.; Li, C. Y. Directed Self-Assembly of Nanoparticles for Nanomotors. *ACS Nano* **2013**, *7*, 5192−5198.

(23) Liu, M.; Liu, L.; Gao, W.; Su, M.; Ge, Y.; Shi, L.; Zhang, H.; Dong, B.; Li, C. Y. A Micromotor Based on Polymer Single Crystals and Nanoparticles: Toward Functional Versatility. *Nanoscale* **2014**, *6*, 8601−8605.

(24) Wu, Z.; Wu, Y.; He, W.; Lin, X.; Sun, J.; He, Q. Self-Propelled Polymer-Based Multilayer Micromotors for Transportation and Drug Release. *Angew. Chem., Int. Ed.* **2013**, *52*, 7000−7003.
(25) Wu, Y.; Wu, Z.; Lin, X.; He, Q.; Li, J. Autonomous Movement of Controllable Assembled Janus Capsule Motors. *ACS Nano* **2012**, *6*, 10910−10916.
(26) Wang, J.; Gao, W. Nano/Microscale Motors: Biomedical Opportunities and Challenges. *ACS Nano* **2012**, *6*, 5745−5751.
(27) Wang, J. Cargo-Towing Synthetic Nanomachines: Towards Active Transport in Microchip Devices. *Lab Chip* **2012**, *12*, 1944−1950.
(28) Campuzano, S.; Orozco, J.; Kagan, D.; Guix, M.; Gao, W.; Sattayasamitsathit, S.; Claussen, J. C.; Merkoci, A.; Wang, J. Bacterial Isolation by Lectin-Modified Microengines. *Nano Lett.* **2012**, *12*, 396−401.
(29) Sanchez, S.; Solovev, A. A.; Schulze, S.; Schmidt, O. G. Controlled Manipulation of Multiple Cells Using Catalytic Microbots. *Chem. Commun.* **2011**, *47*, 698−700.
(30) Kuralay, F.; Sattayasamitsathit, S.; Gao, W.; Uygun, A.; Katzenberg, A.; Wang, J. Self-Propelled Carbohydrate-Sensitive Microtransporters with Built In Boronic Acid Recognition for Isolating Sugars and Cells. *J. Am. Chem. Soc.* **2012**, *134*, 15217−15220.
(31) Guix, M.; Orozco, J.; Garcia, M.; Gao, W.; Sattayasamitsathit, S.; Merkoci, A.; Escarpa, A.; Wang, J. Superhydrophobic Alkanethiol-Coated Microsubmarines for Effective Removal of Oil. *ACS Nano* **2012**, *6*, 4445−4451.
(32) Gao, W.; Kagan, D.; Pak, O. S.; Clawson, C.; Campuzano, S.; Chuluun-Erdene, E.; Shipton, E.; Fullerton, E. E.; Zhang, L.; Lauga, E.; Wang, J. Cargo Towing Fuel-Free Magnetic Nanoswimmers for Targeted Drug Delivery. *Small* **2012**, *8*, 460−467.
(33) Mou, F.; Chen, C.; Zhong, Q.; Yin, Y.; Ma, H.; Guan, J. Autonomous Motion and Temperature-Controlled Drug Delivery of Mg/Pt-poly(N-isopropylacrylamide) Janus Micromotors Driven by Simulated Body Fluid and Blood Plasma. *ACS Appl. Mater. Interfaces* **2014**, *6*, 9897−9903.
(34) Soler, L.; Sanchez, S. Catalytic Nanomotors for Environmental Monitoring and Water Remediation. *Nanoscale* **2014**, *6*, 7175−7182.
(35) Gao, W.; Feng, X.; Pei, A.; Kane, C. R.; Tam, R.; Hennessy, C.; Wang, J. Bioinspired Helical Microswimmers Based on Vascular Plants. *Nano Lett.* **2014**, *14*, 305−310.
(36) He, Q.; Cui, Y.; Ai, S.; Tian, Y.; Li, J. Self-assembly of Composite Nanotubes and Their Applications. *Curr. Opin. Colloid Interface Sci.* **2009**, *14*, 115−125.
(37) Skirtach, A. G.; De Geest, B. G.; Mamedov, A.; Antipov, A. A.; Kotov, N. A.; Sukhorukov, G. B. Ultrasound Stimulated Release and Catalysis Using Polyelectrolyte Multilayer Capsules. *J. Mater. Chem.* **2007**, *17*, 1050−1054.
(38) Gilbert, J. B.; O'Brien, J. S.; Suresh, H. S.; Cohen, R. E.; Rubner, M. F. Orientation-Specific Attachment of Polymeric Microtubes on Cell Surfaces. *Adv. Mater.* **2013**, *25*, 5948−5952.
(39) DeMuth, P. C.; Min, Y.; Huang, B.; Kramer, J. A.; Miller, A. D.; Barouch, D. H.; Hammond, P. T.; Irvine, D. J. Polymer Multilayer Tattooing for Enhanced DNA Vaccination. *Nat. Mater.* **2013**, *12*, 367−376.
(40) Tian, Y.; He, Q.; Cui, Y.; Li, J. Assembled Alginate/chitosan Nanotubes for Biological Application. *Biomacromolecules* **2006**, *7*, 2539−2542.
(41) He, Q.; Tian, Y.; Cui, Y.; Möhwald, H.; Li, J. Layer-by-Layer Assembly of Magnetic Polypeptide Nanotubes as a DNA Carrier. *J. Mater. Chem.* **2008**, *18*, 748−754.
(42) Tabata, Y.; Ikada, Y. Protein Release from Gelatin Matrices. *Adv. Drug Delivery Rev.* **1998**, *31*, 287−301.
(43) Appel, W. Chymotrypsin: Molecular and Catalytic Properties. *Clin. Biochem.* **1986**, *19*, 317−322.
(44) Song, W. X.; Möhwald, H.; Li, J. B. Movement of Polymer Microcarriers Using a Biomolecular Motor. *Biomaterials* **2010**, *31*, 1287−1292.
(45) Sanchez, S.; Solovev, A. A.; Mei, Y. F.; Schmidt, O. G. Dynamics of Biocatalytic Microengines Mediated by Variable Friction Control. *J. Am. Chem. Soc.* **2010**, *132*, 13144−13145.
(46) Gao, W.; Sattayasamitsathit, S.; Uygun, A.; Pei, A.; Ponedal, A.; Wang, J. Polymer-Based Tubular Microbots: Role of Composition and Preparation. *Nanoscale* **2012**, *4*, 2447−2453.
(47) Sheelu, G.; Kavitha, G.; Fadnavis, N. W. Efficient Immobilization of Lecitase in Gelatin Hydrogel and Degumming of Rice Bran Oil Using a Spinning Basket Reactor. *J. Am. Oil. Chem. Soc.* **2008**, *85*, 739−748.
(48) Akkuş Çetinus, Ş.; Nursevin, H. Immobilization of Catalase into Chemically Crosslinked Chitosan Beads. *Enzyme Microb. Technol.* **2003**, *32*, 889−894.
(49) Pigeolet, E.; Corbisier, P.; Houbion, A.; Lambert, D.; Michiels, C.; Raes, M.; Zachary, M.; Remacle, J. Glutathione Peroxidase, Superoxide Dismutase, and Catalase Inactivation by Peroxides and Oxygen Derived Free Radicals. *Mech. Ageing Dev.* **1990**, *51*, 283−297.
(50) Gao, W.; Pei, A.; Wang, J. Water-Driven Micromotors. *ACS Nano* **2012**, *25*, 8432−8438.
(51) Kagan, D.; Benchimol, M. J.; Claussen, J. C.; Chuluun-Erdene, E.; Esener, S.; Wang, J. Acoustic Droplet Vaporization and Propulsion of Perfluorocarbon-Loaded Microbullets for Targeted Tissue Penetration and Deformation. *Angew. Chem., Int. Ed.* **2012**, *124*, 7637−7640.
(52) Sattayasamitsathit, S.; Kou, H.; Gao, W.; Thavarajah, W.; Kaufmann, K.; Zhang, L.; Wang, J. Fully Loaded Micromotors for Combinatorial Delivery and Autonomous Release of Cargoes. *Small* **2014**, *10*, 2830−2833.
(53) Wu, H.; Cao, C.; Kim, J. H.; Hsu, C. H.; Wanebo, H. J.; Bowen, W. D.; Xu, J.; Marshal, J. Trojan-Horse Nanotube On-Command Intracellular Drug Delivery. *Nano Lett.* **2012**, *12*, 5475−5480.